Supplementary Information

Biomimetic MnO_2 Micromotors with Asymmetric Sea Urchin Architecture for Synergistic Mechano-Chemical Eradication of Endodontic Biofilms

Yaping Huang, Jie Li, Qianyang Zhang, Yingjie Wu, Narisu Hu and Sen Mu *a

Supplementary videos

Video S1. Typical video recording of the motors in different concentrations of H_2O_2.

Video S2. Typical video recording of the motors in artificial saliva with 2% H_2O_2.

Video S3. Typical video recording of the motors in saline solution with 2% H_2O_2.

Video S4. Typical video recordings of motor enter root canal side branches in simulated root canal environments.

Supplementary Figures

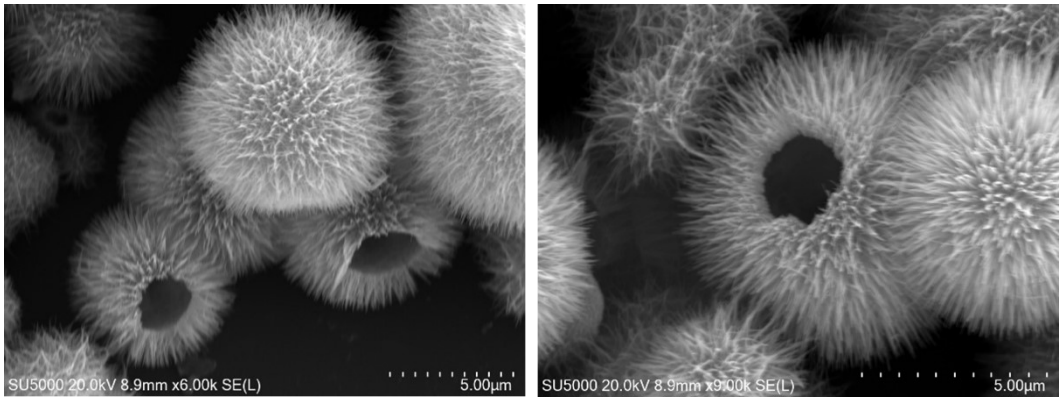

Figure S1 SEM images of multiple manganese dioxide micromotors in the same field of view.

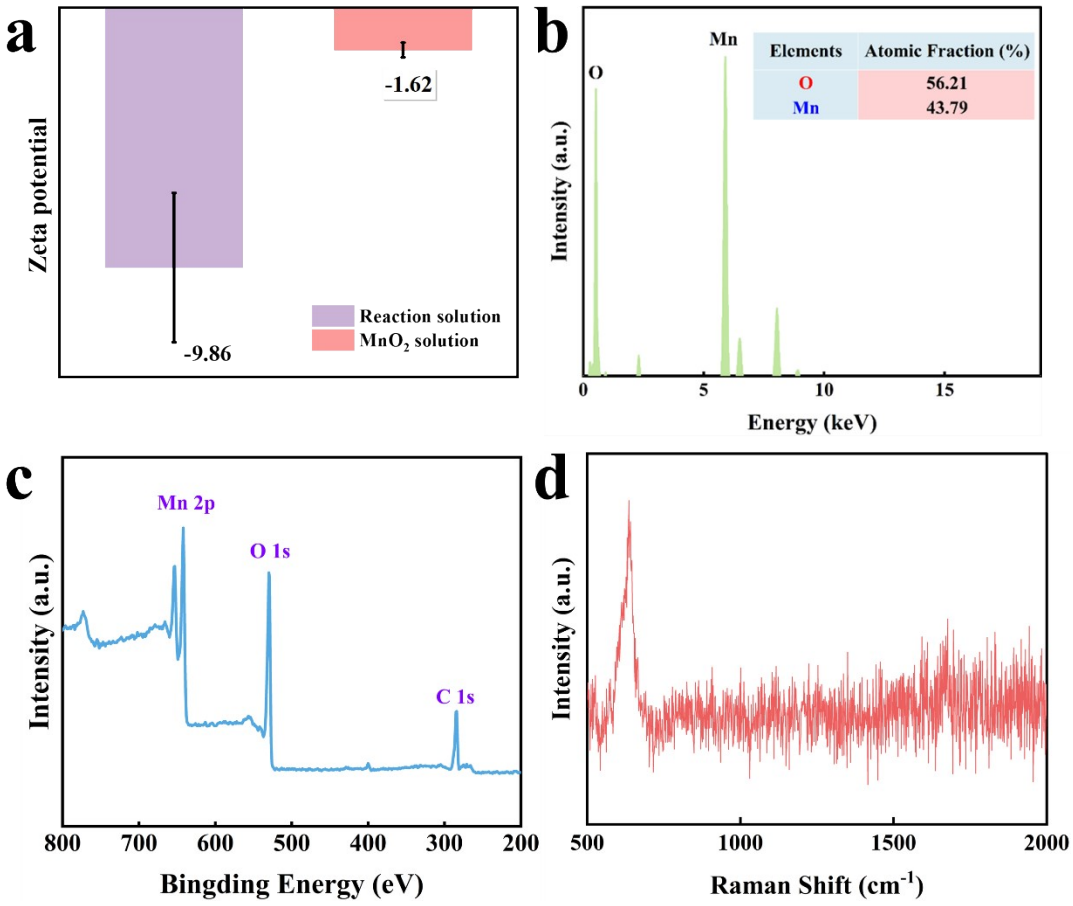

Figure S2. (a)Comparison of zeta potential images of the pre-reaction and post-reaction solutions of manganese dioxide micromotors. (b) Elemental composition analysis of manganese dioxide micromotors. (c) XPS full spectrum analysis of manganese dioxide micromotors. (d) In situ Raman testing of manganese dioxide micromotors.

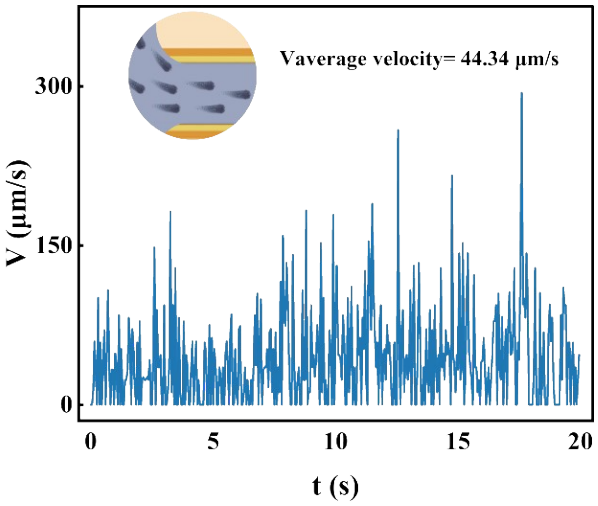

Figure S3. V-T diagram of a manganese dioxide micromotor in a simulated root canal, with an average velocity of 44.34 μm/s. (The inset shows a schematic diagram of the simulated motor moving in the root canal)

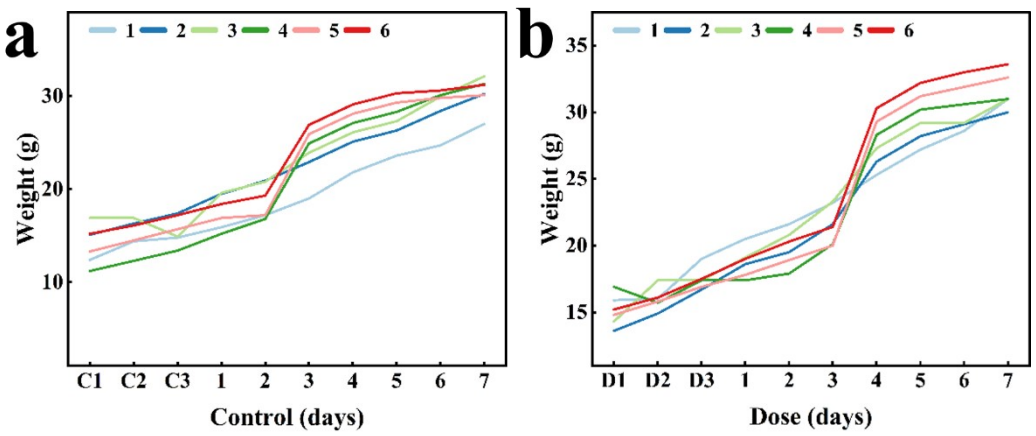

Figure S4. (a) Curve showing changes in mouse weight over time under normal feeding conditions. (b) Curve showing changes in mouse weight over time under conditions of manganese dioxide gavage.

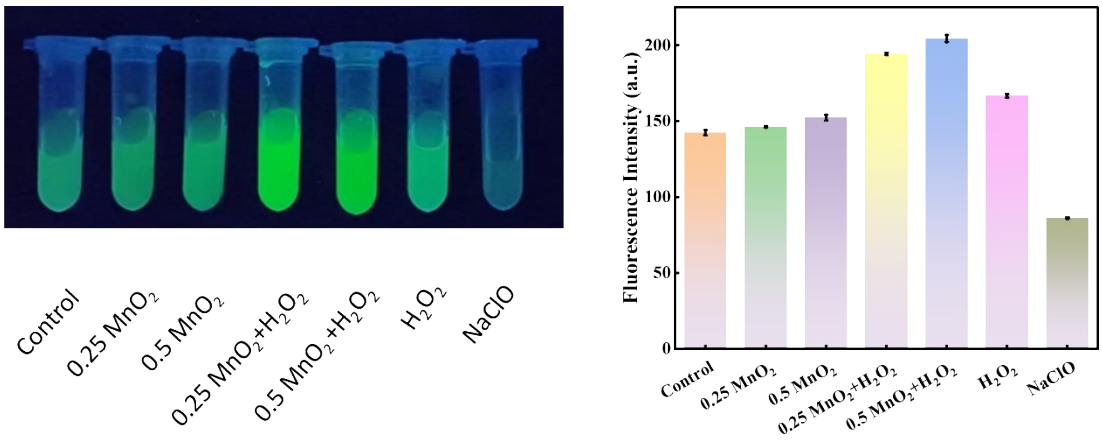

Figure S5 Comparison of reactive oxygen species (ROS) fluorescence intensity among different experimental groups. The left panel displays the DCFH-DA fluorescence signals corresponding to each experimental group, while the right panel quantitatively characterizes the fluorescence intensity of different groups, presented as mean ± standard deviation (n = 3).

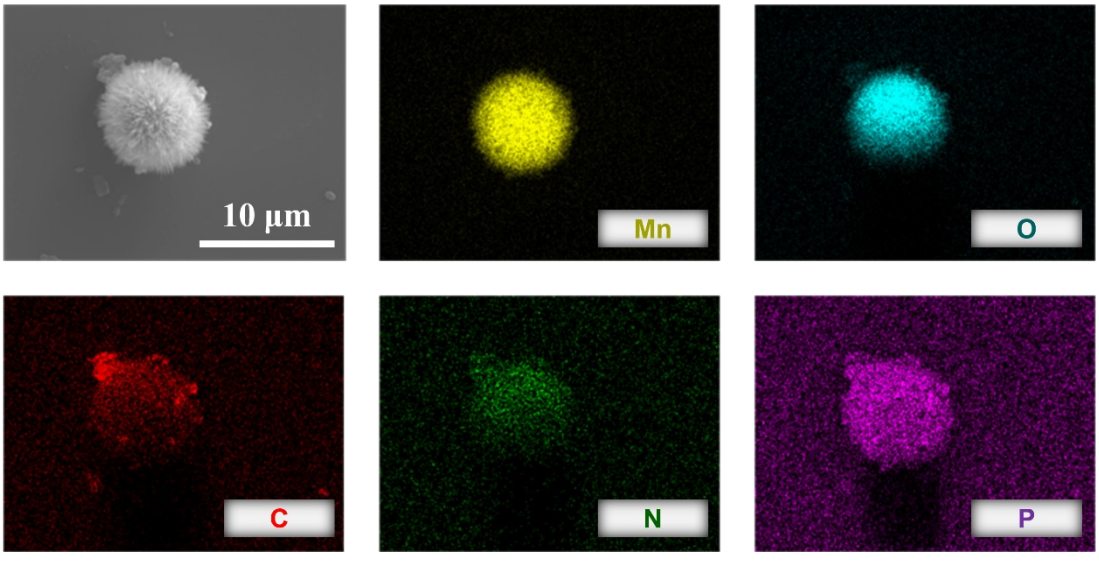

Figure S6 SEM characterization of MnO_2 micromotors after co-cultivation with Enterococcus faecalis. Elemental analysis indicates that the micromotors are tightly adhered to the bacteria.

Supplementary text

To rigorously evaluate the mechanical disruption capability of our MnO_2 micromotors, we conducted a systematic stress analysis at the micromotor-bacteria interface.

Fundamental Parameters:
Micromotor Geometry: Needle tip radius (r) = 7.18 ± 1.52 nm (from SEM measurements), length ≈500 nm (SEM)
Bacterial Membrane: Young's modulus (E) = 10 MPa ((literature value for E. faecalis), Poisson's ratio (ν) = 0.5
Contact angle (θ): ~30° (from TEM image analysis)

Thrust Force Generation:
The propulsion force is calculated using Stokes' drag for spherical micromotors:

$F = 6\pi\eta R v = 6\pi \times 0.001 Pa \cdot s \times 3\mu m \times 33.8\mu m/s = 1.9 nN$
where η is water viscosity, R is micromotor radius, and v is measured velocity.

Contact Mechanics Analysis:

The effective modulus combines bacterial membrane properties:
$$E^* = \frac{E}{1-\nu^2} = \frac{10}{1-0.5^2} MPa = 13.3 MPa$$

Applying Hertz contact theory for a spherical tip
$$a = \left(\frac{3Fr}{4E^*}\right)^{1/3} = \left(\frac{3(1.9nN)(7.18nm)}{4(13.3MPa)}\right)^{1/3} = 9.3nm$$

The maximum contact stress becomes
$$\sigma_{max} = \frac{3F}{2\pi a^2} = \frac{3(1.9nN)}{2\pi(9.3nm)^2} = 10.5MPa$$

Stress Concentration Enhancement:
The needle geometry amplifies stress at the tip:
$$SCF = 1 + 2\sqrt{\frac{L}{r}} = 1 + 2\sqrt{\frac{500}{7.18}} \approx 17.7$$
$$\sigma_{effective} = SCF \times \sigma_{max} = 17.7 \times 10.5 MPa = 186 MPa$$

The calculated effective stress of 186 MPa far exceeds the 10-50 MPa rupture threshold of bacterial membranes, demonstrating that the sharp needle geometry enables sufficient stress concentration for mechanical disruption. This physical penetration effect, as clearly observed in SEM images (Fig. 4b), works synergistically with the chemical ROS attack to enhance antibacterial action. The quantitative stress analysis thus confirms that our micromotors' nanoscale needle tips can mechanically compromise bacterial membranes while substantiating their dual mechano-chemical

antibacterial mechanism.

The references for calculating the relevant parameters are as follows:

1. N. S. Zhang, J. X. Yan, M. Y. Wang, X. H. Li, H. T. Shen, M. M. Lv, M. L. Wu, J. W. Zhang and S. Y. Li, Electrochimica Acta, 2025, 536.
2. J. Lee, K. Jha, C. E. Harper, W. Y. Zhang, M. Ramsukh, N. Bouklas, T. Dörr, P. Chen and C. J. Hernandez, Acs Biomaterials Science & Engineering, 2024, 10, 2956-2966.
3. M. Li, C. Y. Gan, W. X. Shao, C. Yu, X. G. Wang and Y. Chen, Scanning, 2016, 38, 70-79.